Supporting Information

Redox and "Antioxidant" Properties of $Fe_2(\mu\text{-}SH)_2(CO)_4(PPh_3)_2$

Husain N. Kagalwala, Noemie Lalaoui, Qian-Li Li, Liang Liu,
Toby Woods, and Thomas B. Rauchfuss*
School of Chemical Sciences
University of Illinois
Urbana, IL 61801, USA

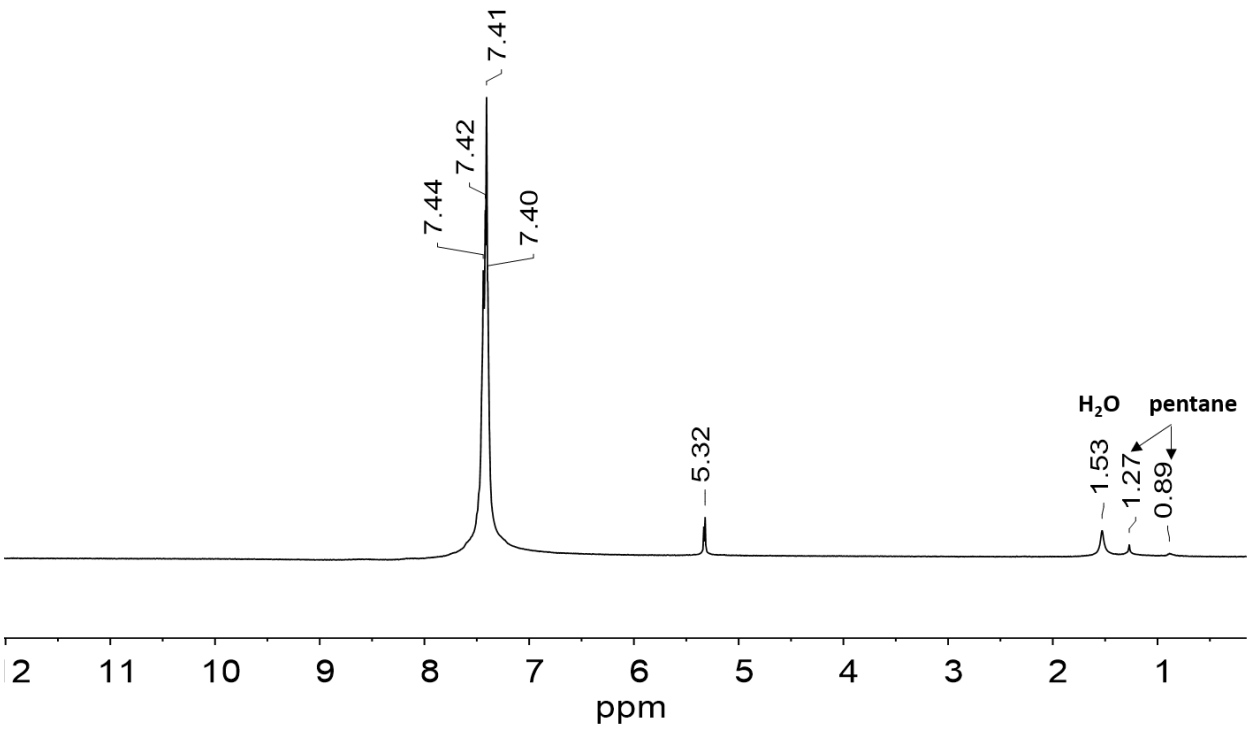

Figure S1. ^1H NMR spectrum (500 MHz, CD_2Cl_2) of $Fe_2(\mu\text{-}S_2)(CO)_4(PPh_3)_2$ at 20 ºC.

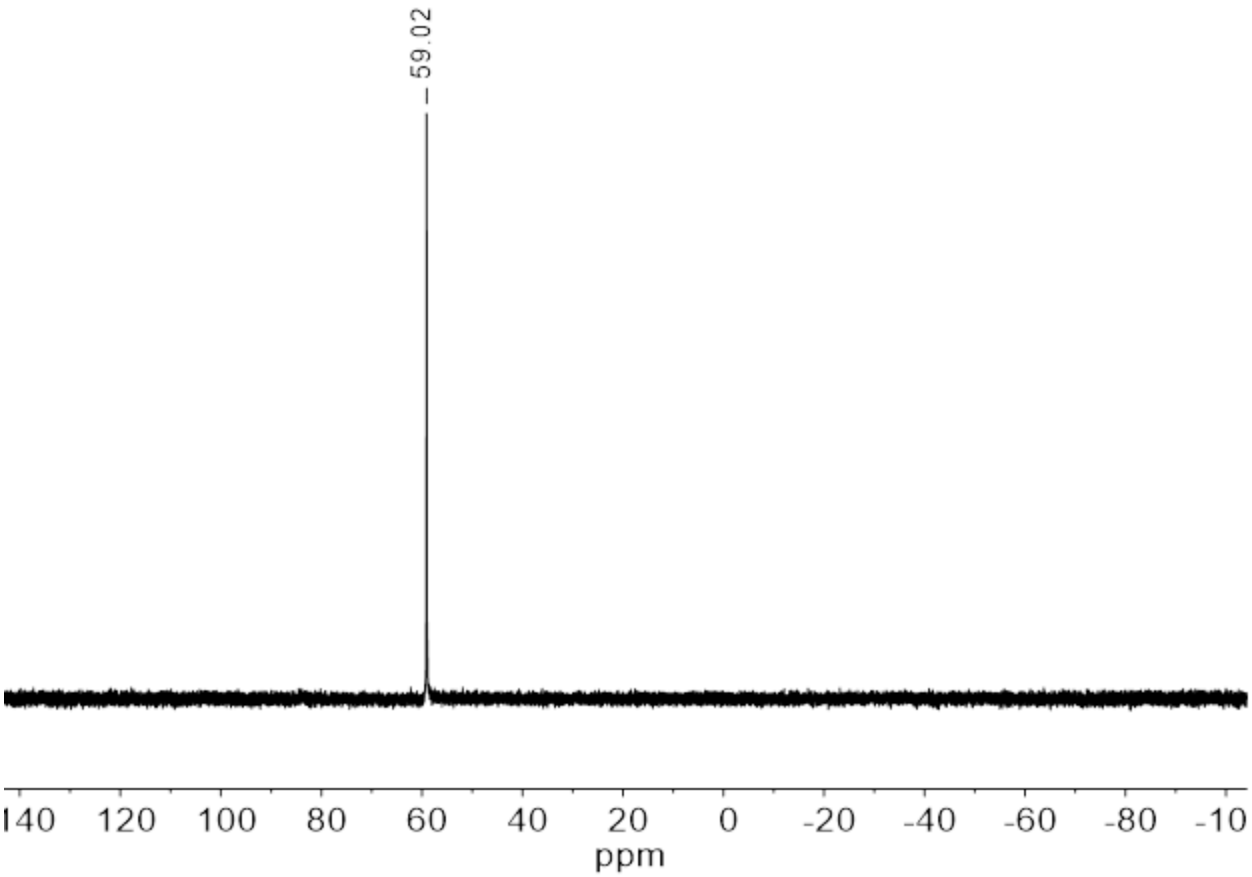

Figure S2. ^{31}P NMR spectrum (202 MHz, CD_2Cl_2) of $Fe_2(\mu\text{-}S_2)(CO)_4(PPh_3)_2$ at 20 ºC.

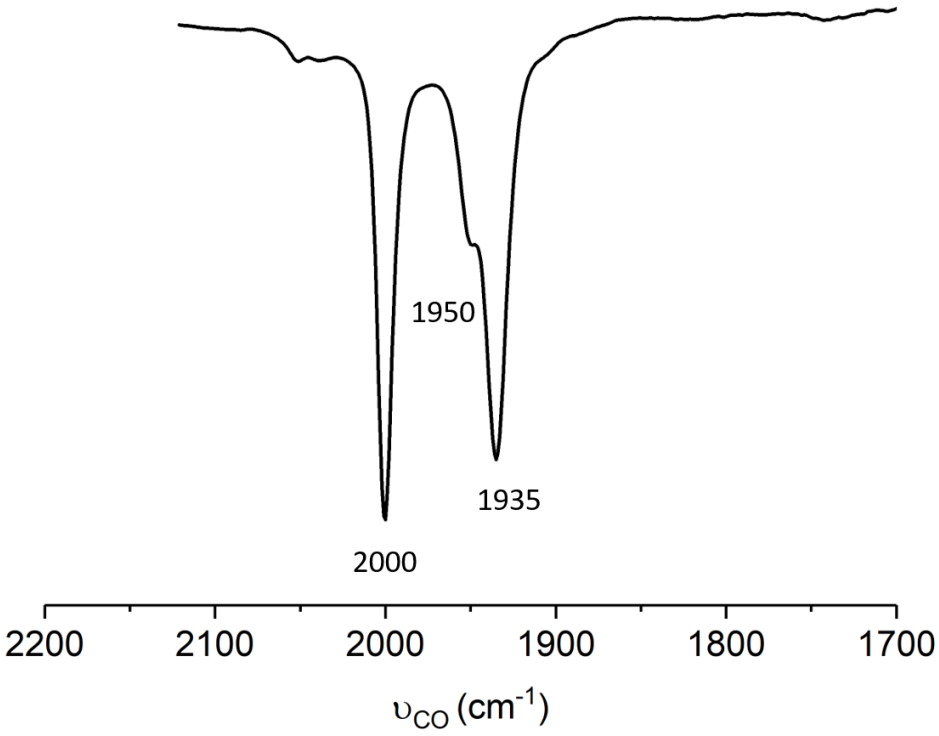

Figure S3. IR spectrum of $Fe_2(\mu\text{-}S_2)(CO)_4(PPh_3)_2$ in CH_2Cl_2 solution (20 ºC).

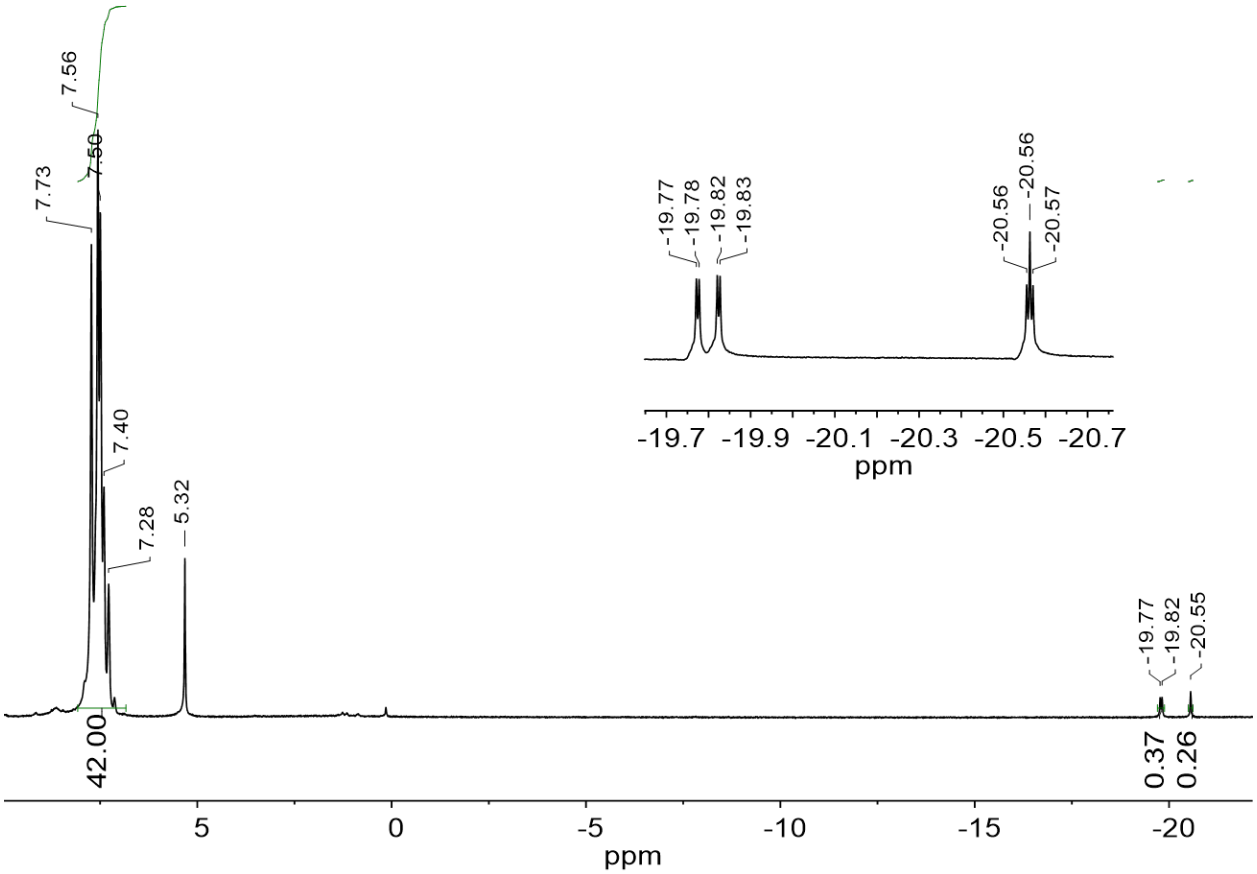

Figure S4. ^{1}H NMR spectrum (500 MHz, CD_2Cl_2) of $[(\mu\text{-H})Fe_2(\mu\text{-}S_2)(CO)_4(PPh_3)_2]BAr^F{}_4$ at 20 ºC. *Inset:* expansion of high field region.

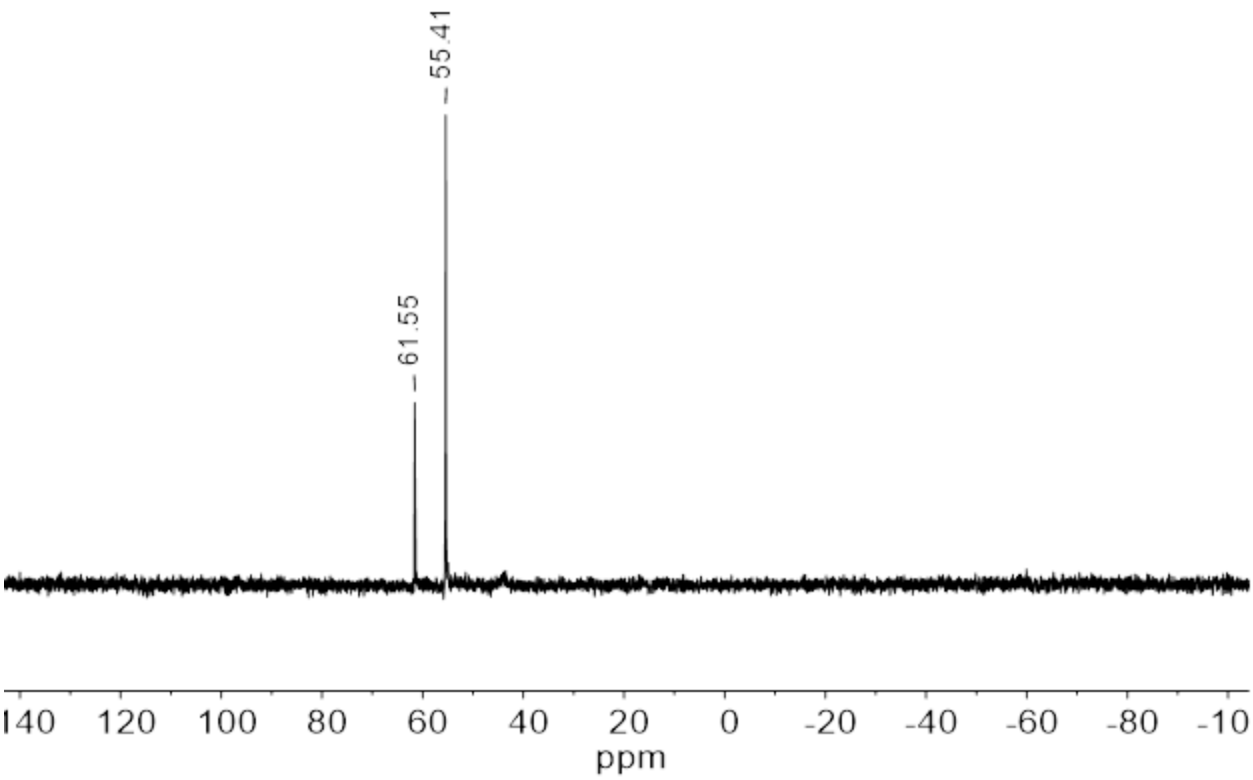

Figure S5. ^{31}P NMR spectrum (202 MHz, CD_2Cl_2) of $[(\mu\text{-}H)Fe_2(\mu\text{-}S_2)(CO)_4(PPh_3)_2]BAr^F{}_4$ at 20 ºC.

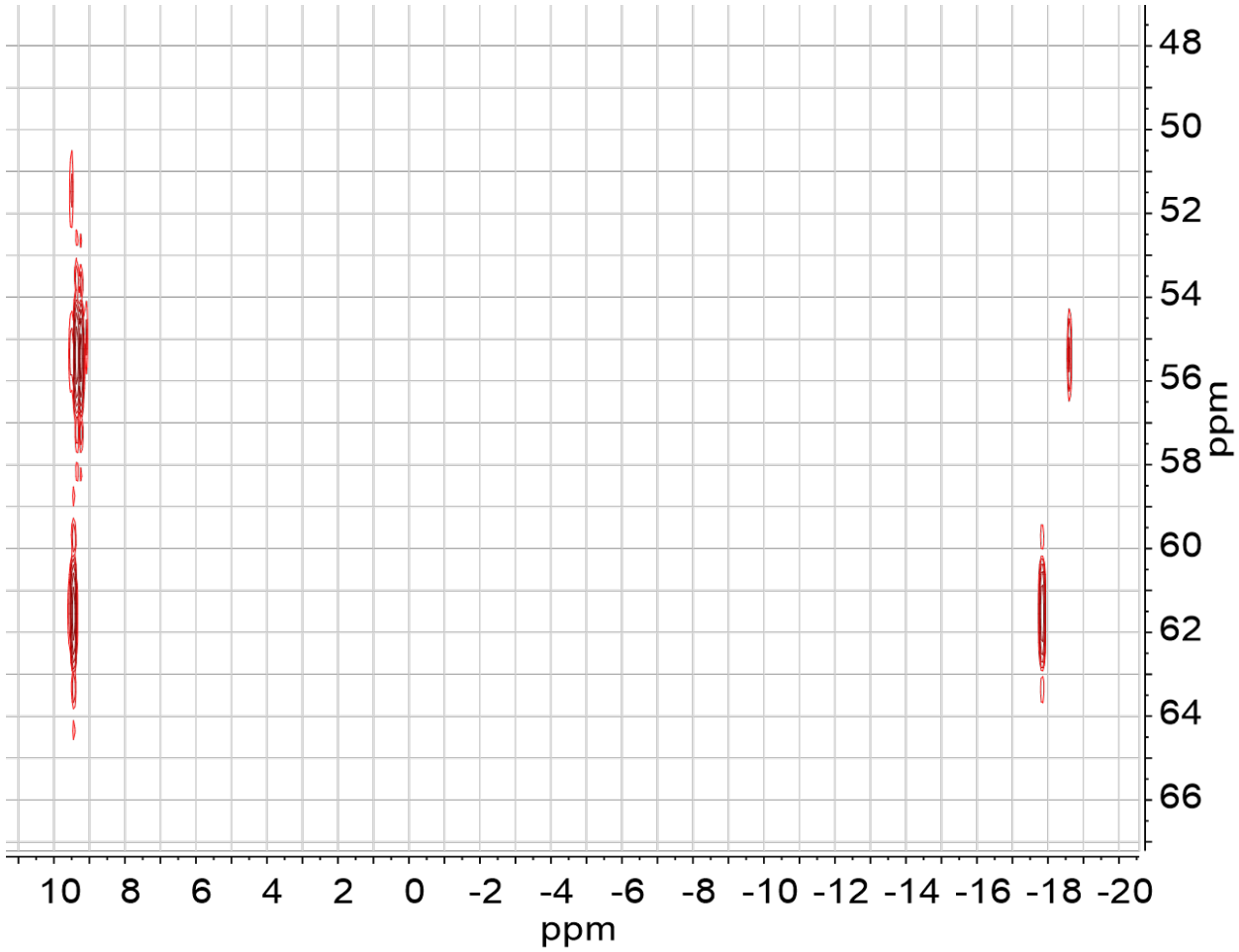

Figure S6. ^{1}H-^{31}P HMBC spectrum of $[(\mu\text{-}H)Fe_2(\mu\text{-}S_2)(CO)_4(PPh_3)_2]BAr^F{}_4$ at 20 ºC.

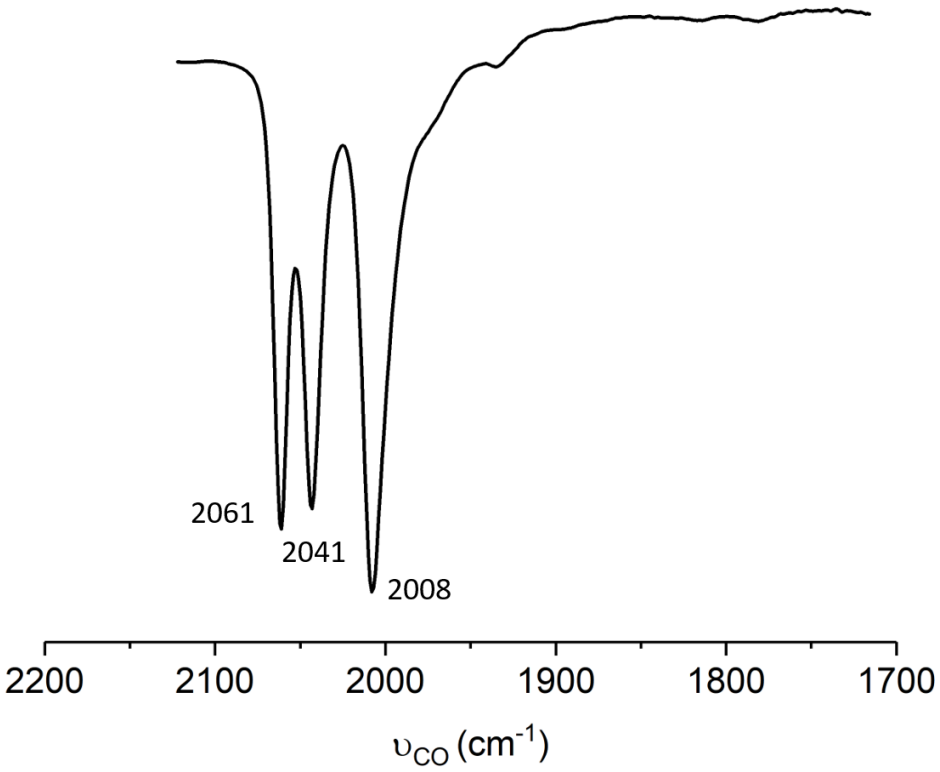

Figure S7. IR spectrum in CH_2Cl_2 solution of $[(\mu\text{-H})Fe_2(\mu\text{-}S_2)(CO)_4(PPh_3)_2]BAr^F{}_4$ at 20 ºC.

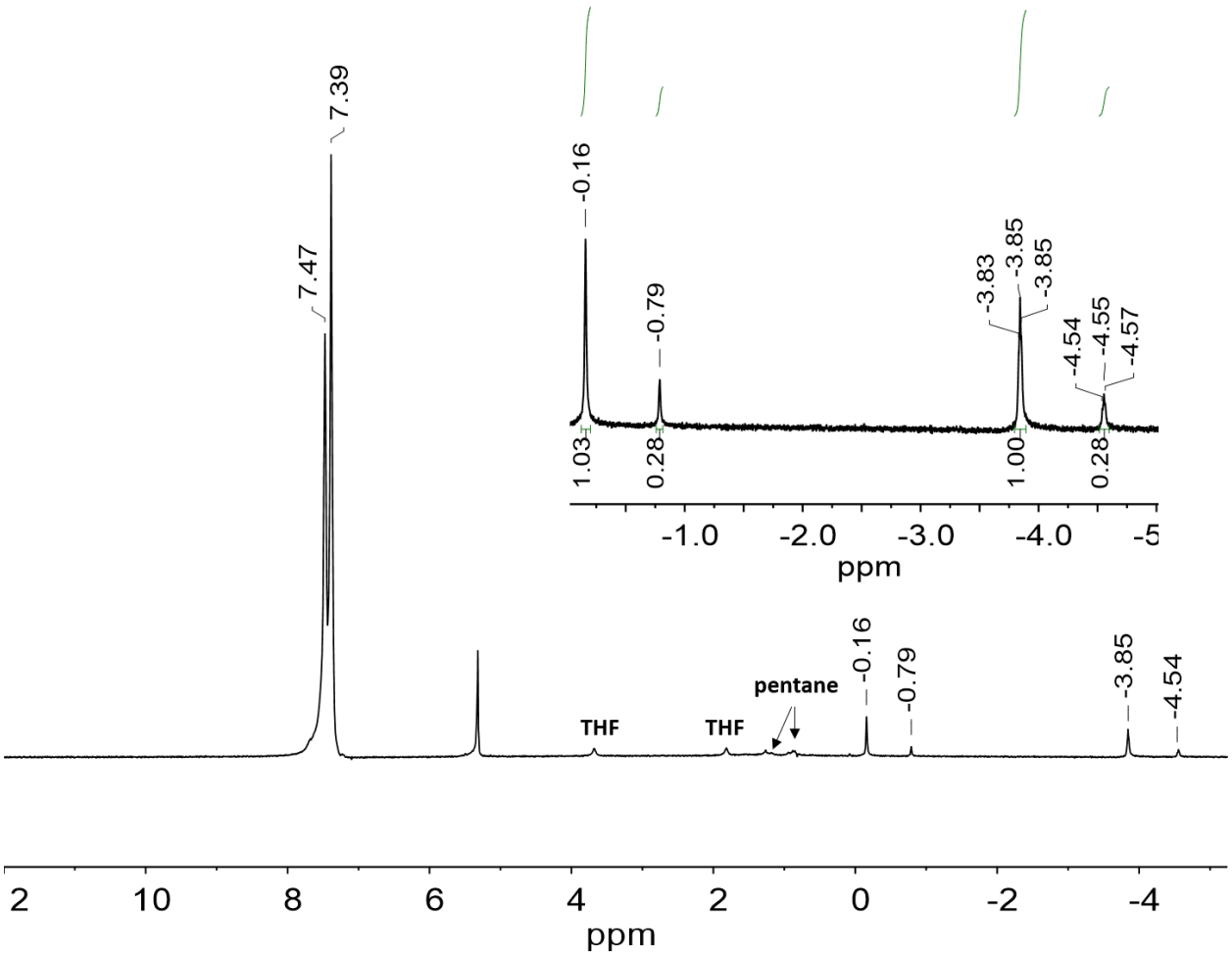

Figure S8. ^{1}H NMR spectrum (500 MHz, CD_2Cl_2) of $Fe_2(\mu\text{-}SH)_2(CO)_4(PPh_3)_2$ at 20 ºC.

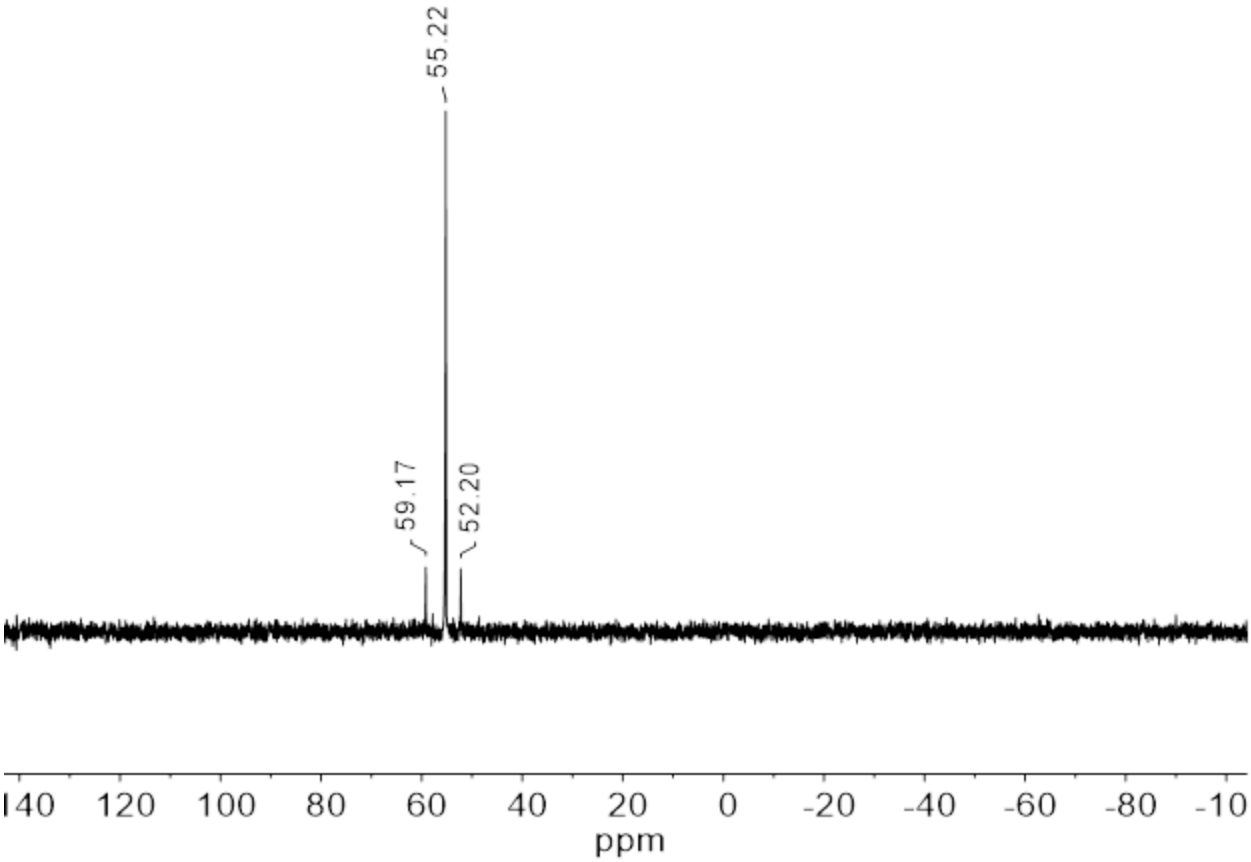

Figure S9. ^{31}P NMR spectrum (202 MHz, CD_2Cl_2) of $Fe_2(\mu\text{-}SH)_2(CO)_4(PPh_3)_2$ at 20 ºC.

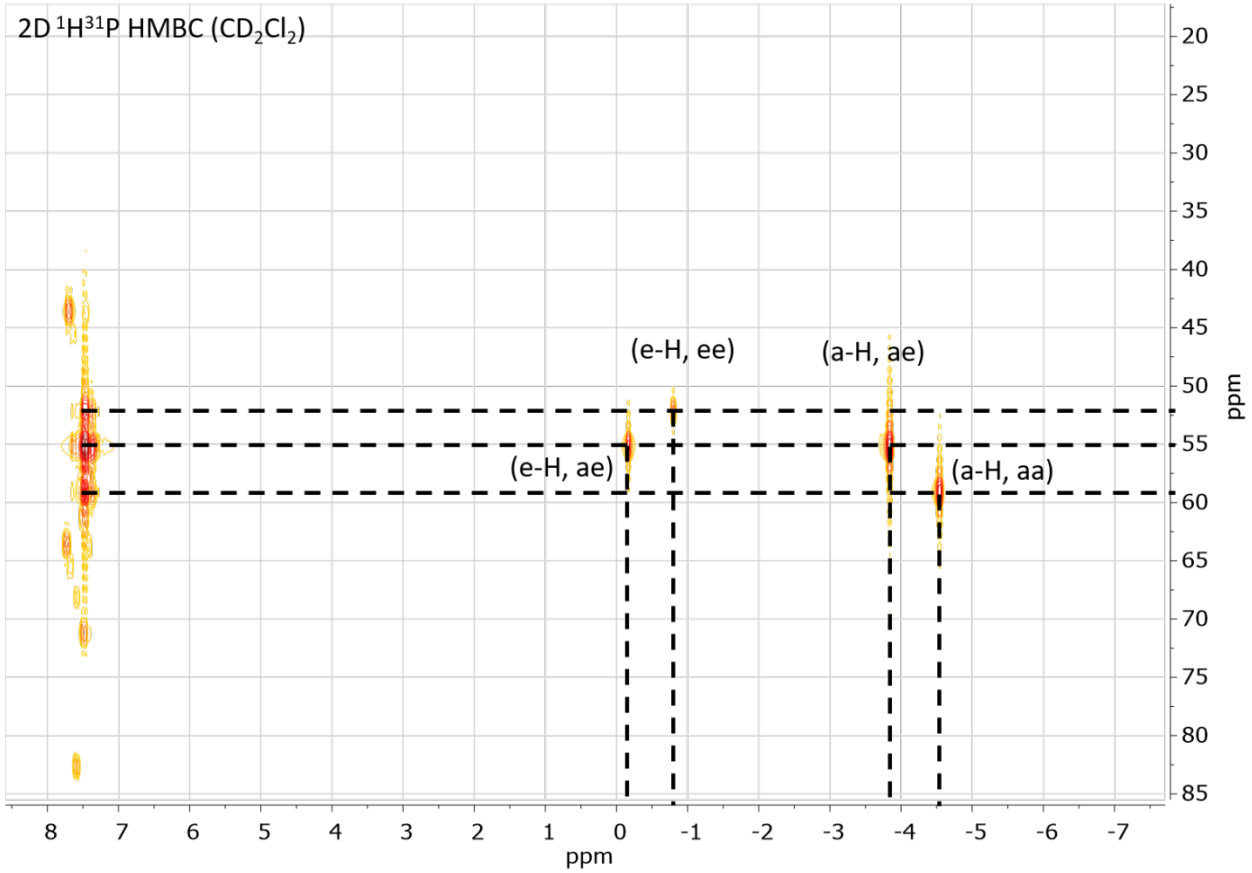

Figure S10. ^{1}H-^{31}P HMBC spectrum of $Fe_2(\mu\text{-}SH)_2(CO)_4(PPh_3)_2$ at 20 ºC.

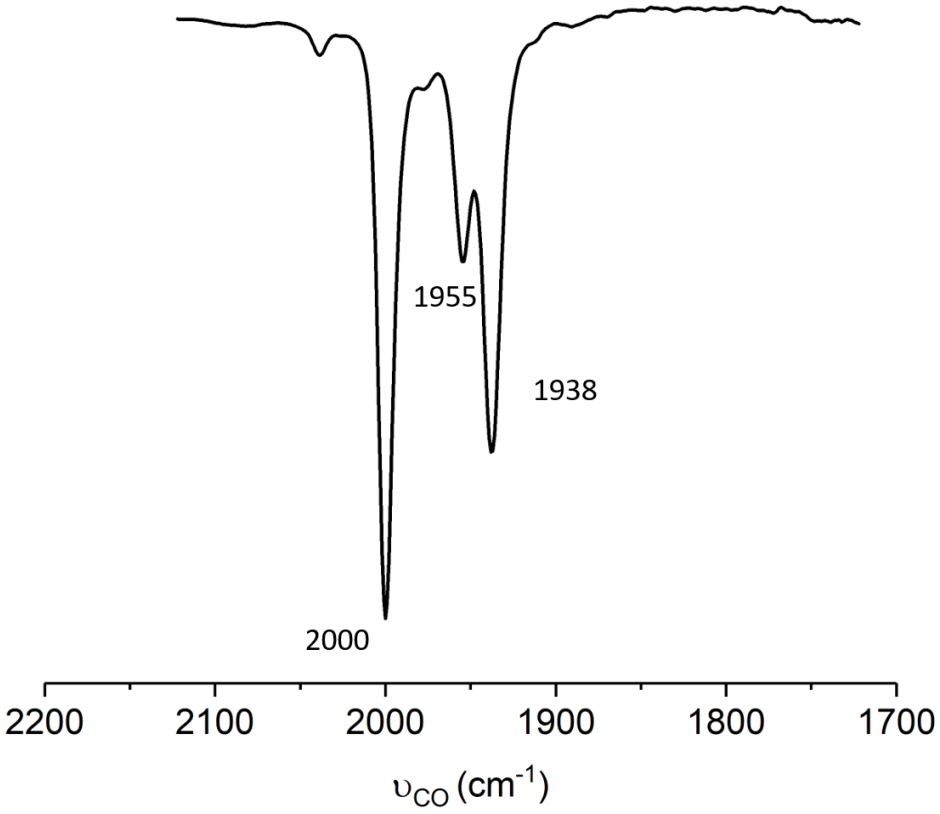

Figure S11. IR spectrum in CH_2Cl_2 of $Fe_2(\mu\text{-}SH)_2(CO)_4(PPh_3)_2$ at 20 ºC.

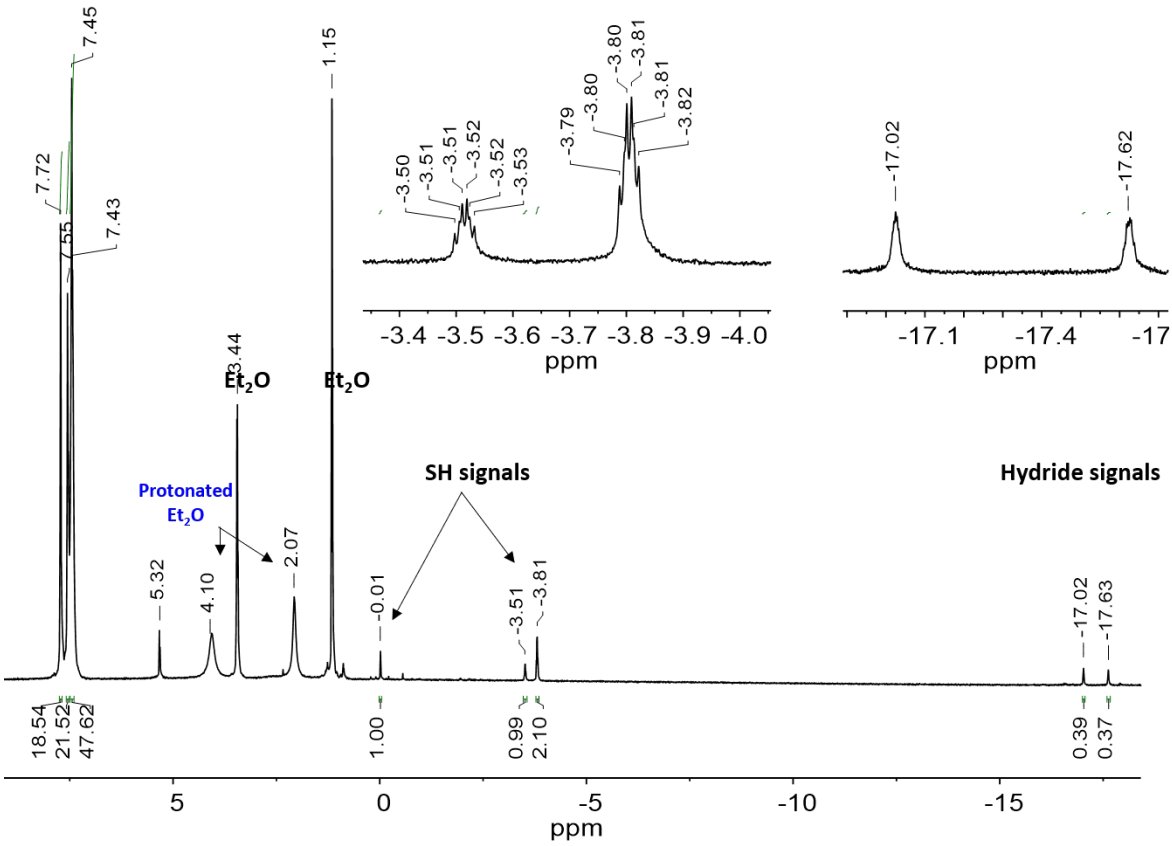

Figure S12. ^{1}H NMR spectrum (500 MHz, CD_2Cl_2) of $[(\mu\text{-}H)Fe_2(\mu\text{-}SH)_2(CO)_4(PPh_3)_2]BAr^F{}_4$ (generated *in situ*) at -20 ºC. The hydride signals indicate approximately 1:1 isomer ratio.

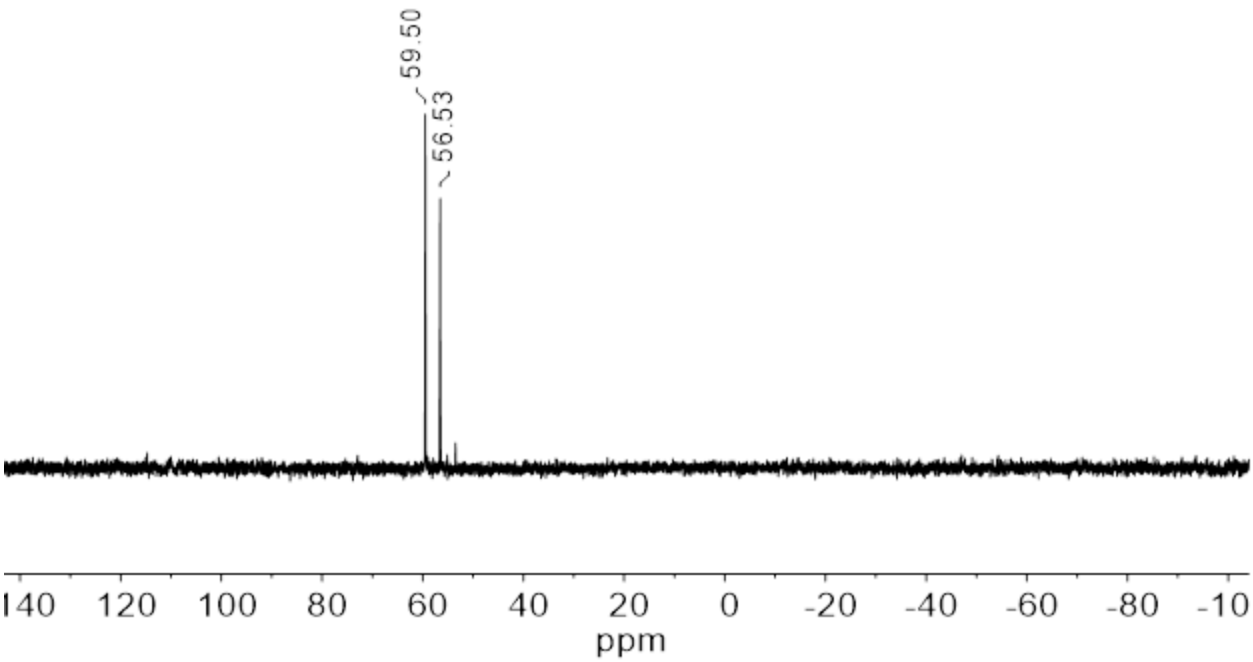

Figure S13. ^{31}P NMR spectrum (202 MHz, CD_2Cl_2) of $[(\mu\text{-}H)Fe_2(\mu\text{-}SH)_2(CO)_4(PPh_3)_2]BAr^F{}_4$ (generated *in situ*) at -20 ºC.

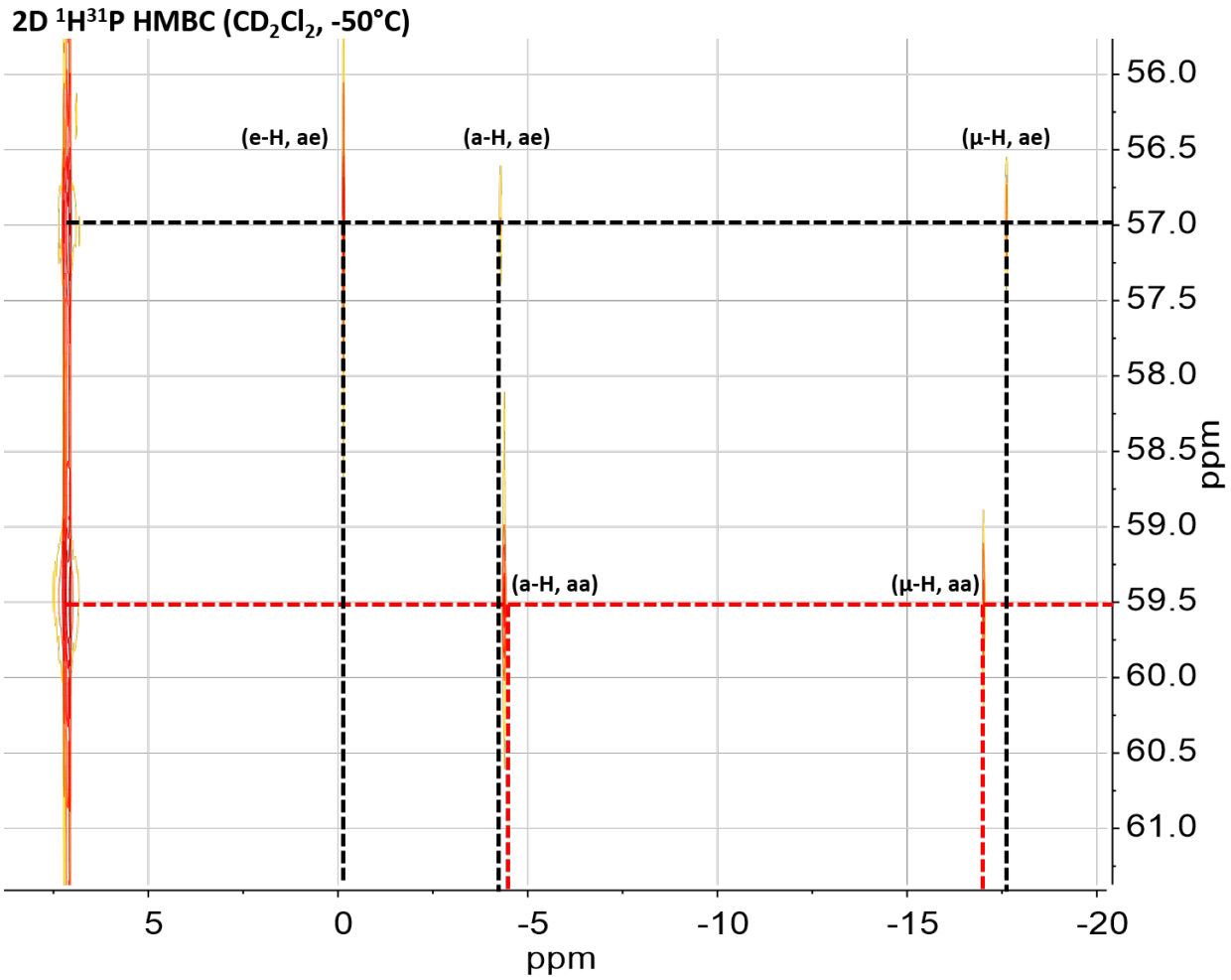

Figure S14. ^{1}H-^{31}P HMBC spectrum of $[(\mu\text{-}H)Fe_2(\mu\text{-}SH)_2(CO)_4(PPh_3)_2]BAr^F{}_4$ (generated *in situ*) at -50 ºC.

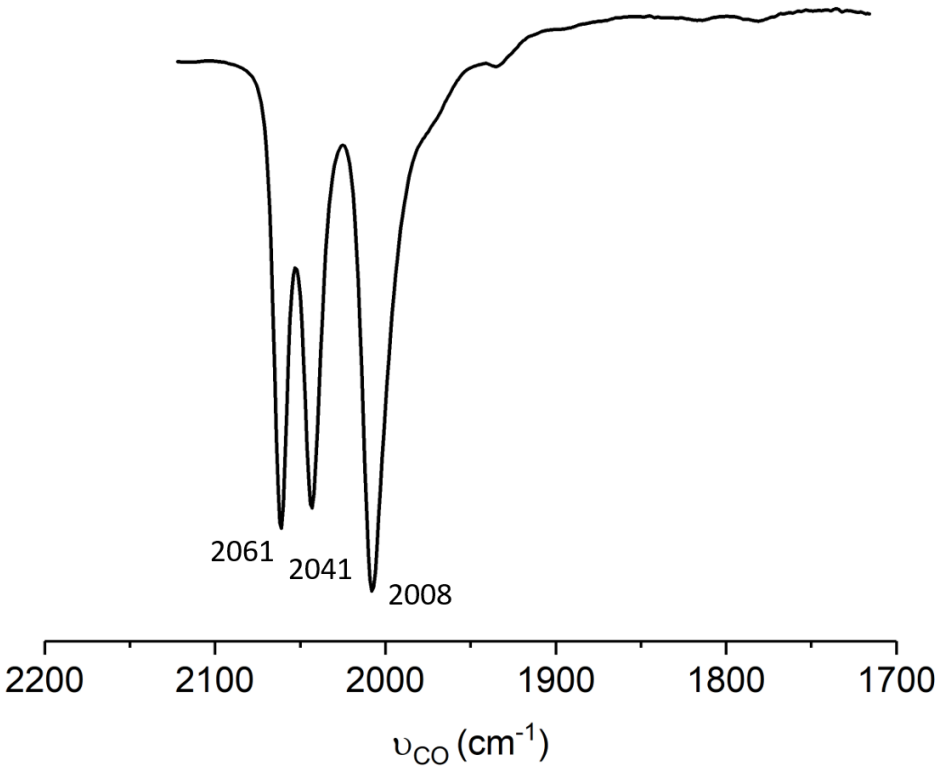

Figure S15. IR spectrum of a CH_2Cl_2 solution of $[(\mu\text{-}H)Fe_2(\mu\text{-}SH)_2(CO)_4(PPh_3)_2]BAr^F{}_4$ at 20 ºC.

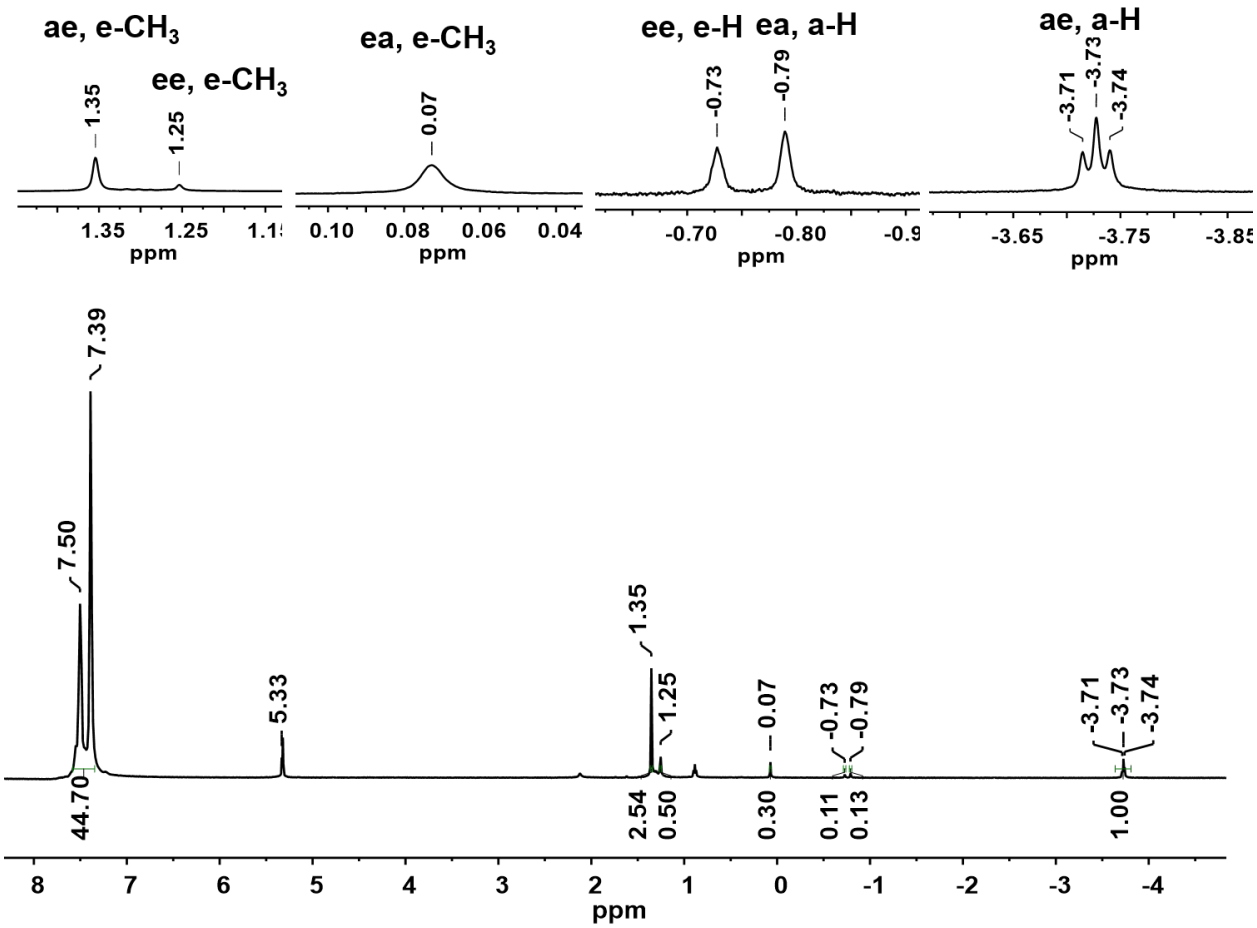

Figure S16. ^{1}H NMR spectrum (500 MHz, CD_2Cl_2) of $Fe_2(\mu\text{-SMe})(\mu\text{-SH})(CO)_4(PPh_3)_2$ at 20 ºC. *Inset:* expansion of S*Me* and S*H* signals.

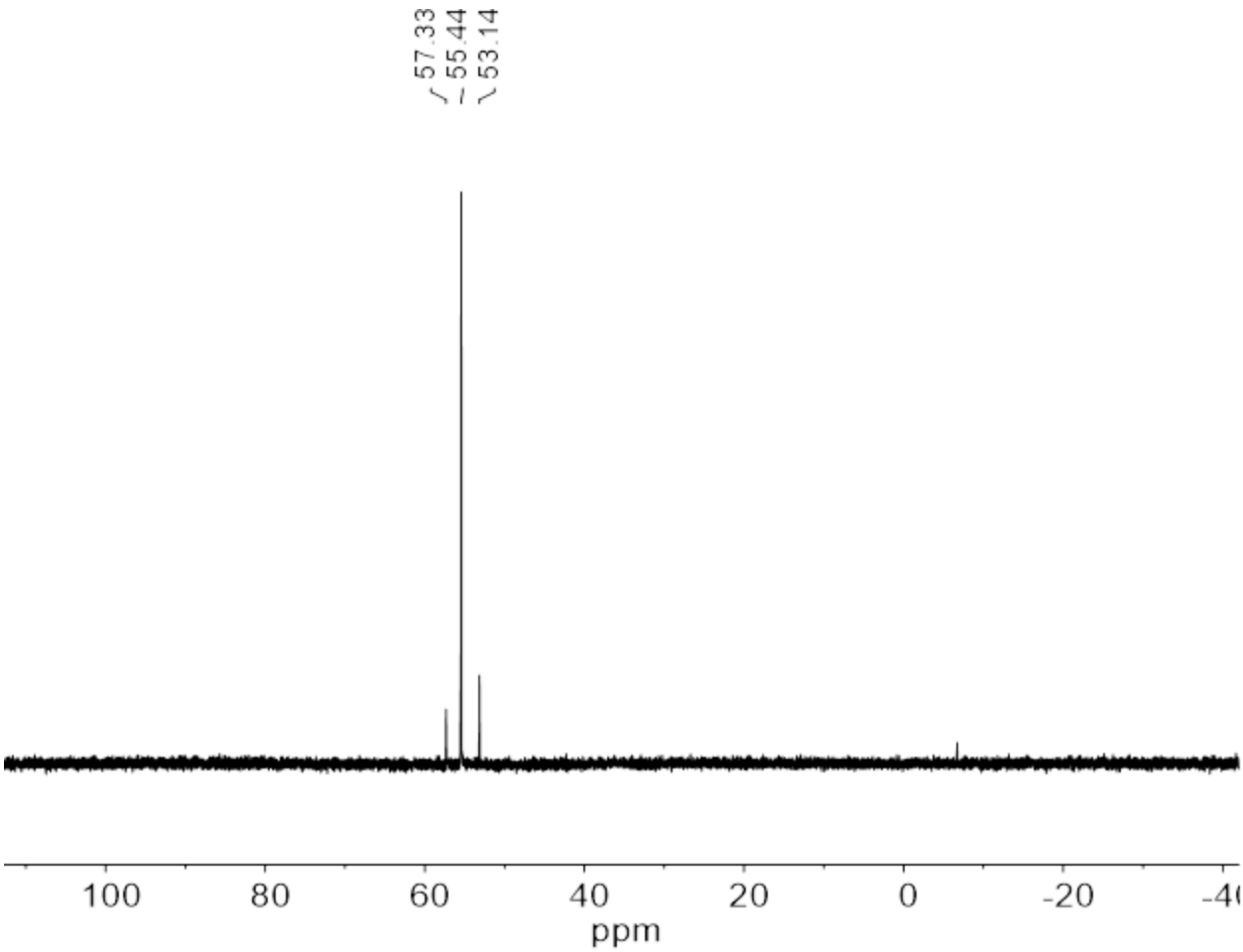

Figure S17. ^{31}P NMR spectrum (202 MHz, CD_2Cl_2) of $Fe_2(\mu\text{-SMe})(\mu\text{-SH})(CO)_4(PPh_3)_2$ at 20 ºC.

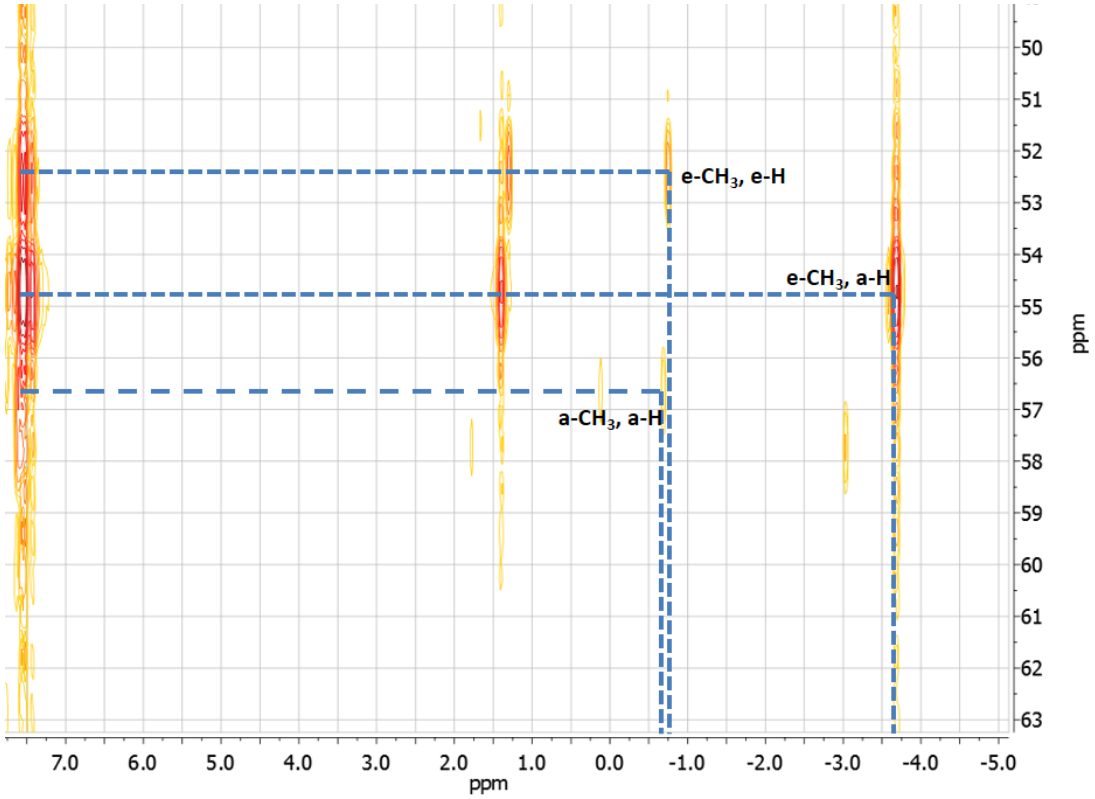

Figure S18. ^{1}H-^{31}P HMBC spectrum of $Fe_2(SMe)(SH)(CO)_4(PPh_3)_2$ at 20 ºC.

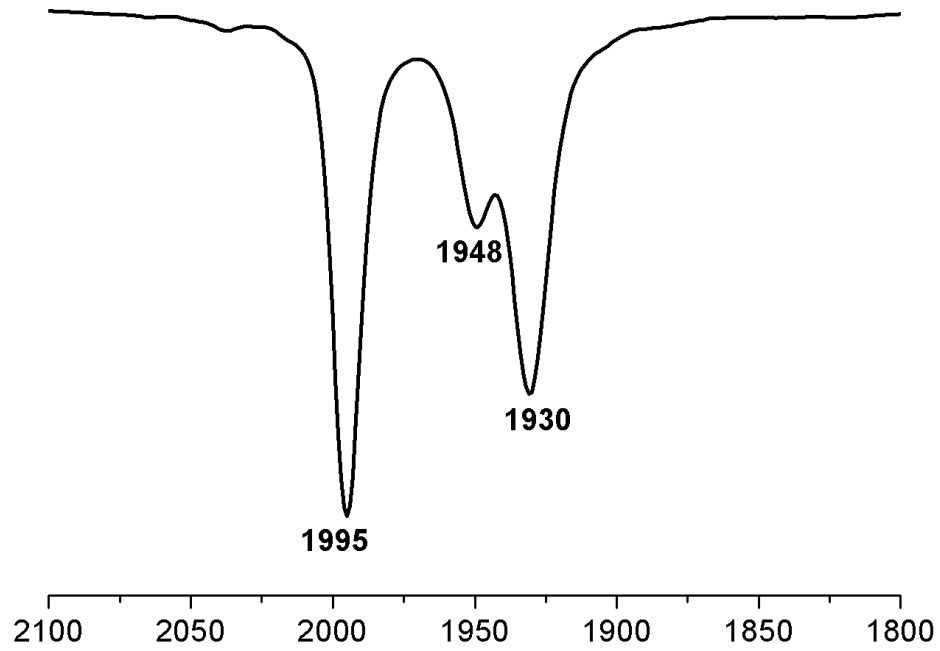

Figure S19. IR spectrum of a CH_2Cl_2 solution of $Fe_2(\mu\text{-SMe})(\mu\text{-SH})(CO)_4(PPh_3)_2$ at 20 ºC.

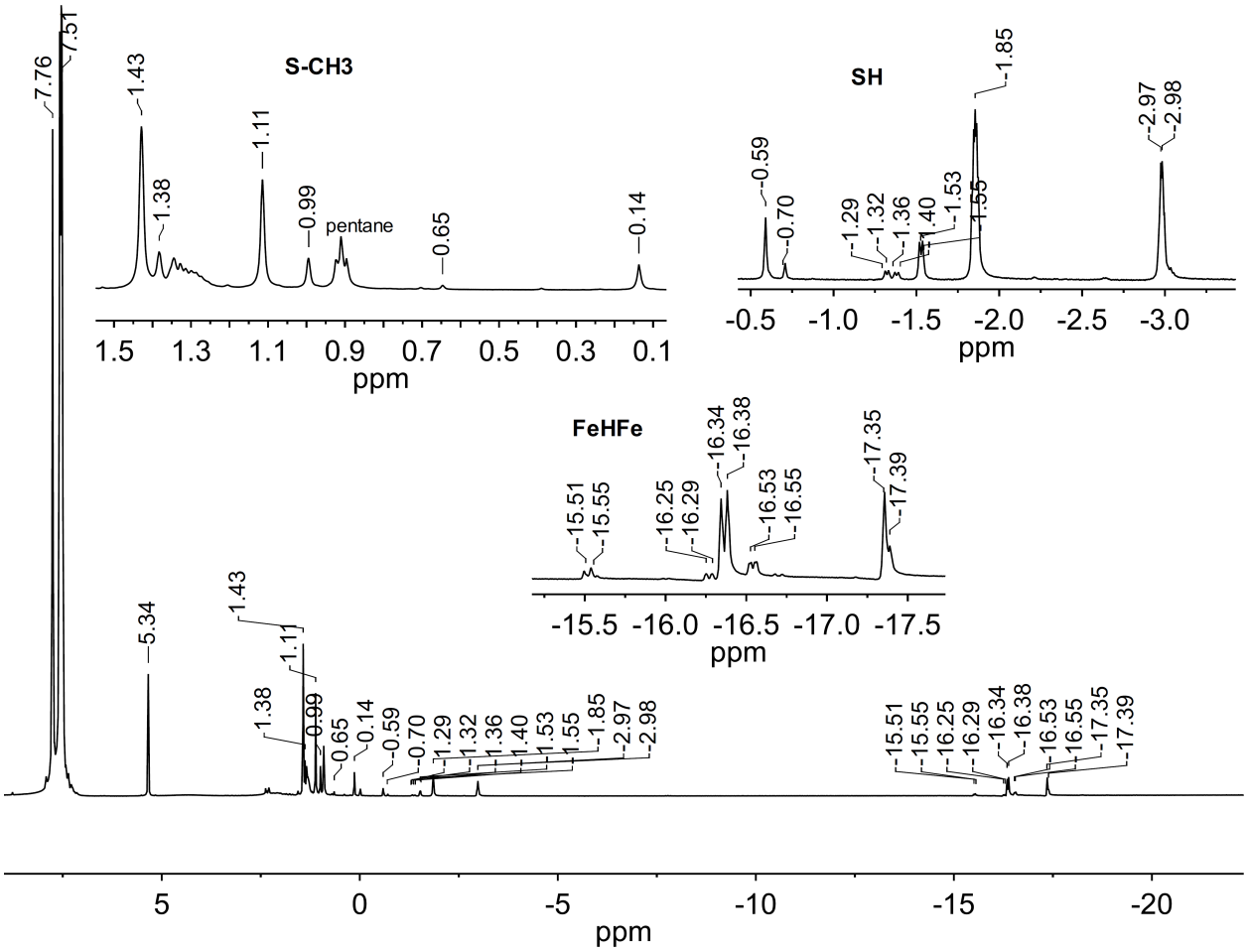

Figure S20. ^{1}H NMR spectrum (500 MHz, CD_2Cl_2) of [(μ-H)Fe_2(μ-SMe)(μ-SH)$(CO)_4(PPh_3)_2$]$BAr^F{}_4$ at 20 ºC. *Insets:* expansions of the spectra in the S*Me*, S*H*, and Fe*H* regions.

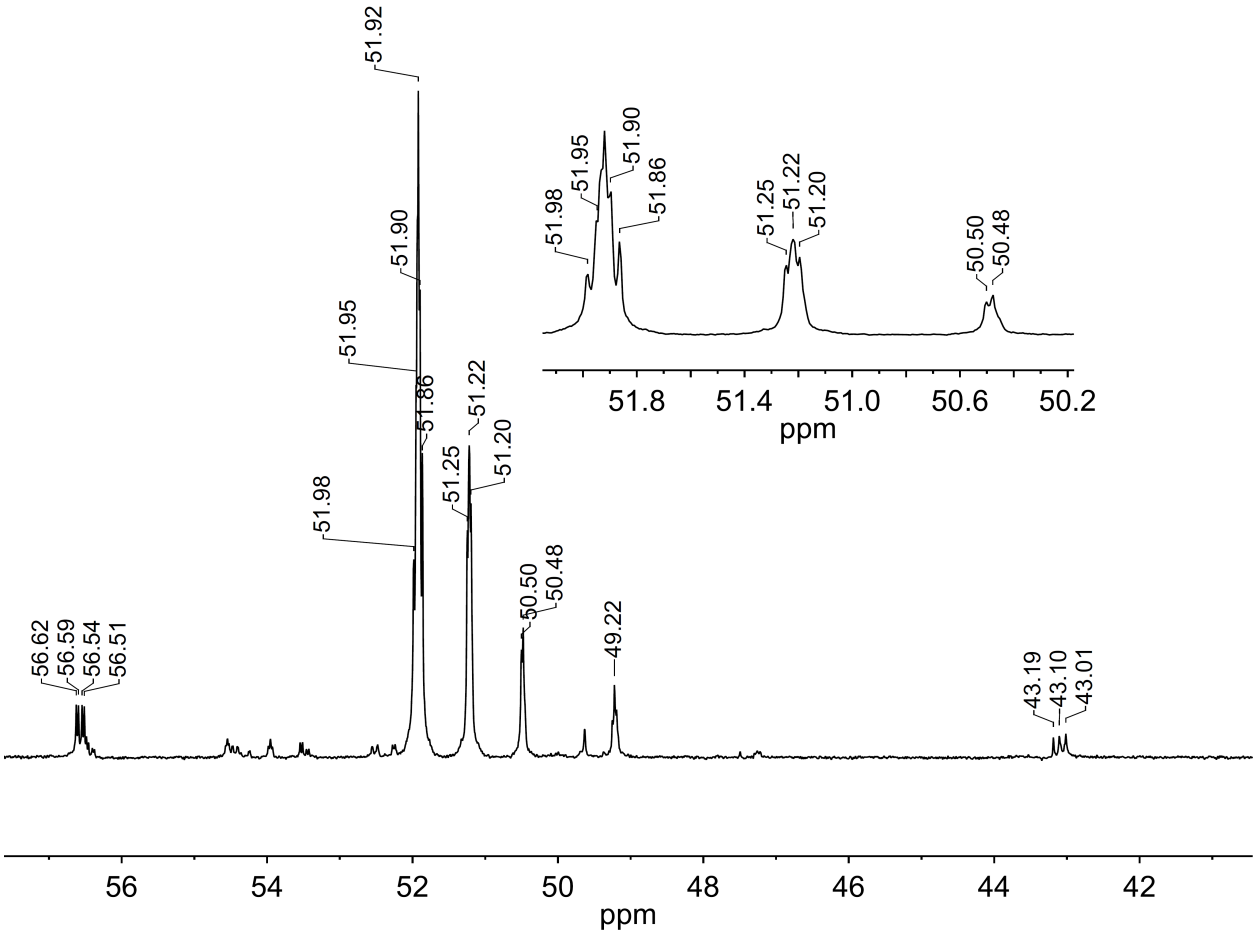

Figure S21. ^{31}P NMR spectrum (202 MHz, CD_2Cl_2) of $[(\mu\text{-H})Fe_2(\mu\text{-SMe})(\mu\text{-SH})(CO)_4(PPh_3)_2]BAr^F{}_4$ at 20 ºC.

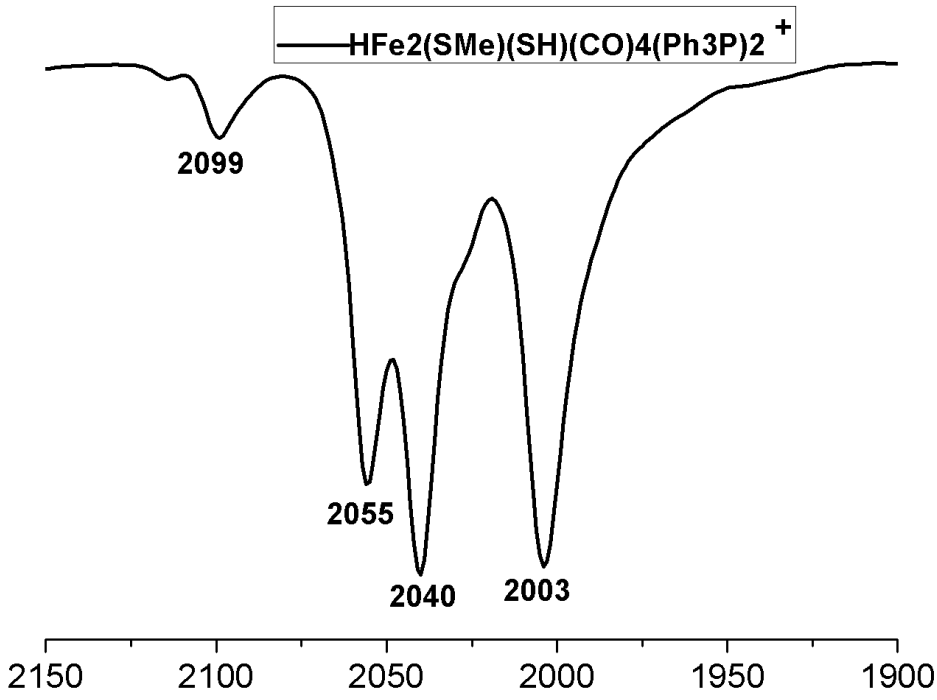

Figure S22. IR spectrum of CH_2Cl_2 solution of [(μ-H)Fe_2(μ-SMe)(μ-SH)$(CO)_4(PPh_3)_2$]$BAr^F{}_4$ at 20 ºC.

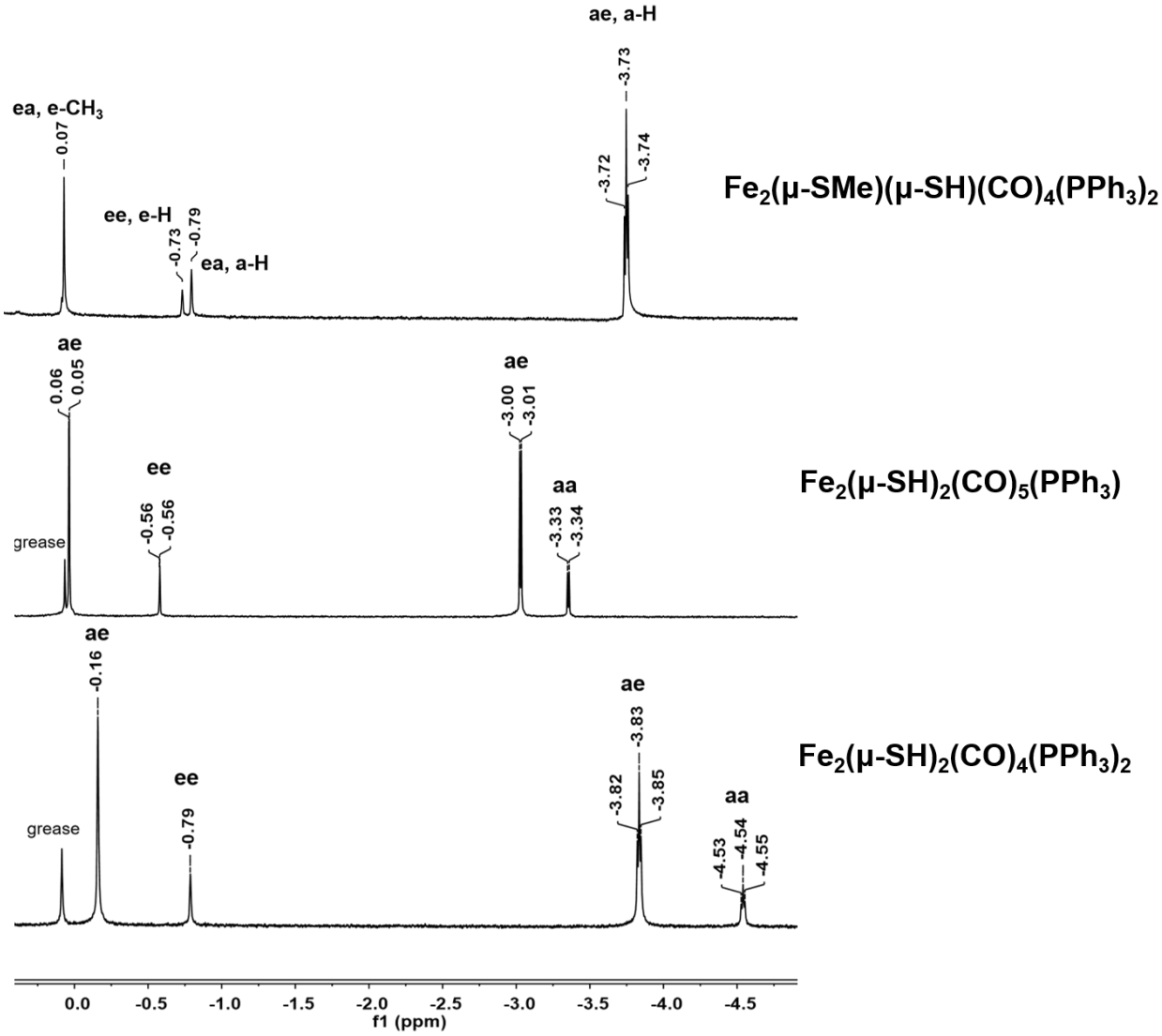

Figure S23. ^{1}H NMR spectra (500 MHz, CD_2Cl_2) of $Fe_2(\mu\text{-}SR)_2(CO)_{6-x}(PPh_3)_x$ derivatives (R = H, Me), depicting the μ-SH signals.

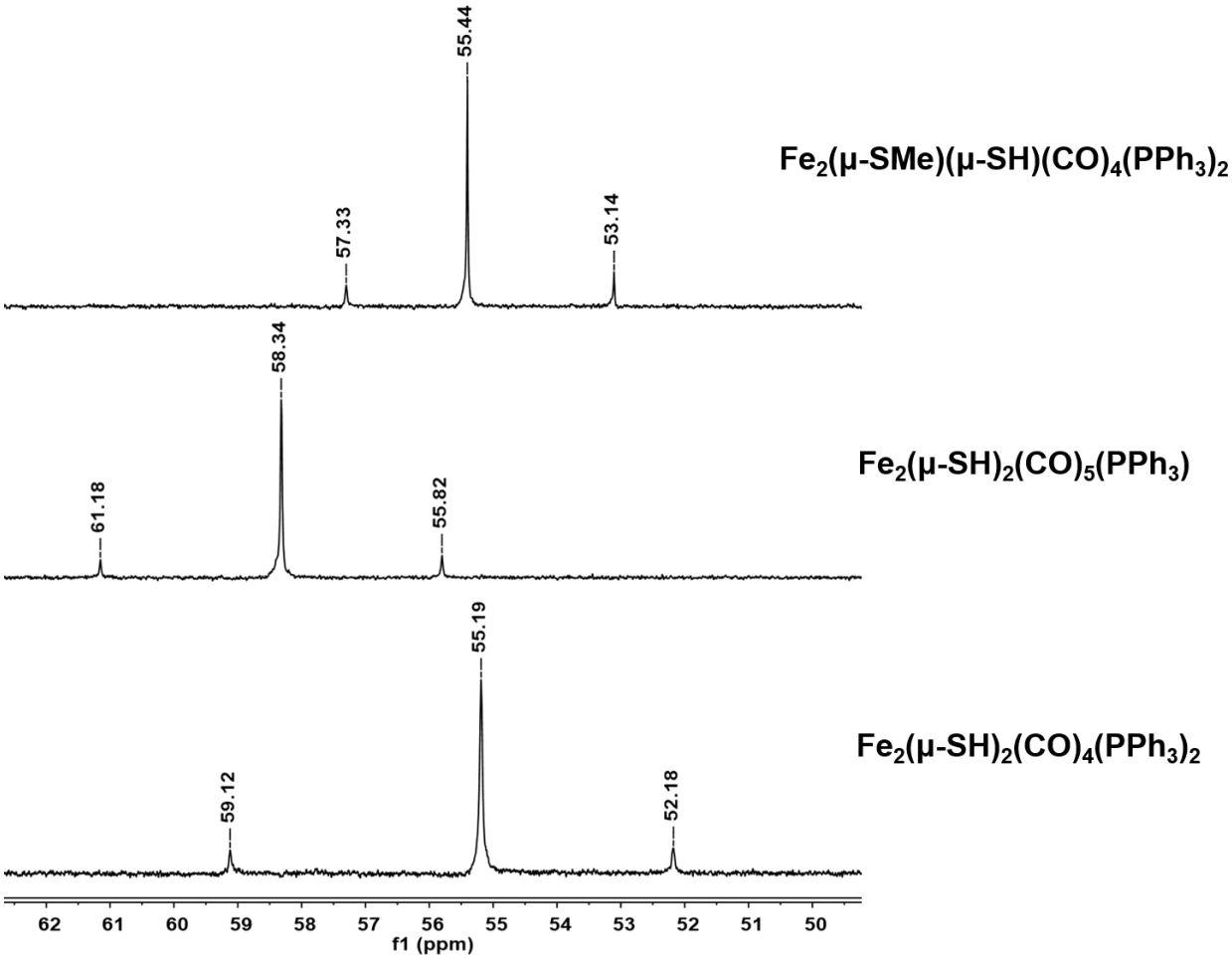

Figure S24. ^{31}P NMR spectra (202 MHz, CD_2Cl_2) of $Fe_2(\mu\text{-}SR)_2(CO)_{6-x}(PPh_3)_x$ derivatives (R = H, Me).

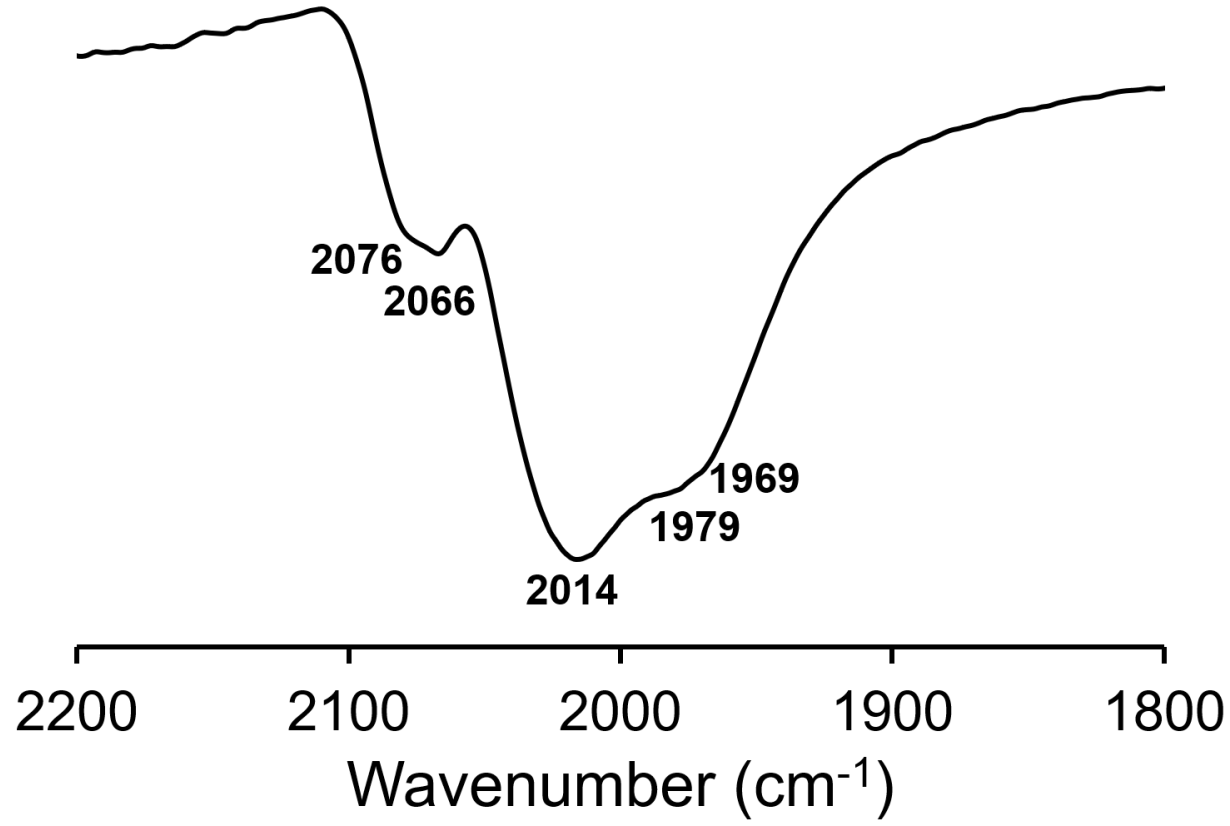

Figure S25. Reflectance IR spectrum of the black solid generated from the reaction of $\mathbf{1}^{HH}$ with 2 equiv TEMPO in THF solution.

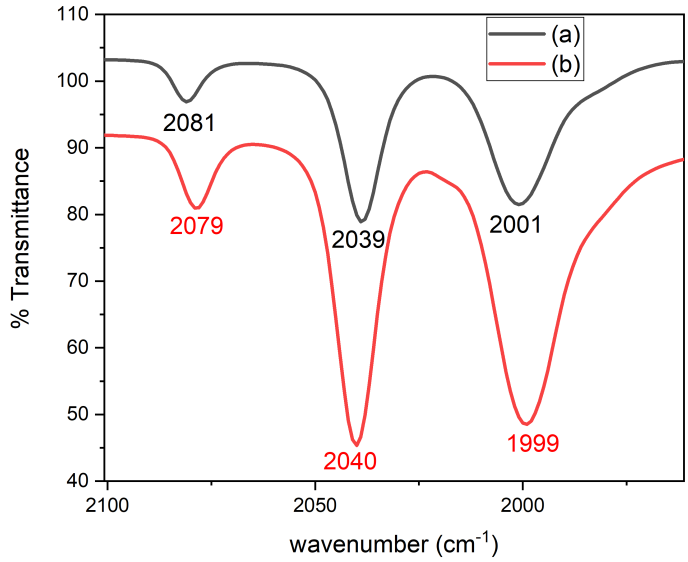

Figure S26. IR spectra of THF solutions of (a) **1** (b) $\mathbf{1}^{HH}$.